A CINEMATOGRAPHIC INVESTIGATION OF CRACK GROWTH THE DOUBLE-TORSION TESTING OF POLYMERS:

R.Frassine, T.Riccò, M.Rink, A.Pavan*

The double - torsion test is a convenient and straightforward method of characterizing the fracture behaviour of rate-sensitive materials. Real-time visualization of the curved-crack growth developed in this test provides information towards an insight into the kinematics and dynamics of the fracture process. This enables requirements for the applicability of the conventional double-torsion analysis to be outlined.

INTRODUCTION

Interest in the double-torsion (DT) test stems from the combination of experimental simplicity with the possibility of determining the fracture resistance of rate-sensitive materials.

The specimen consists of a rectangular plate, side-grooved to prevent crack wandering and edge-notched at the end of the specimen where the load is applied (see Fig. 1a). The four-point loading system generates torsion on each of the two rectangular beams, separated by the notch.

The two torsional beams are not ideally clamped at their ends, since the uncracked portion of the plate is compliant; however, conventional "pure torsion" analysis (Timoshenko and Goodier (1)) has been satisfactorily applied to this test configuration. From that analysis, the specimen compliance, C, is expressed by:

*Dipartimento di Chimica Industriale e Ingegneria Chimica "G.Natta" Politecnico di Milano

$$C = \frac{2(1+\nu)l^2}{k_1 E W B^3} a + Co \qquad (1)$$

which indicates the "linear compliance" characteristic of this test. The critical strain energy release rate can be expressed in terms of compliance as:

$$G_c = \frac{P_c^2}{2} \frac{(dC/da)}{(dA/da)} \qquad (2)$$

If the crack profile does not change with crack extension, it can be shown that:

$$\frac{dA}{da} = B_c \qquad (3)$$

Combination of equations (1), (2) and (3) gives (Kies and Clark (2), Evans (3), Marshall and al.(4), Beaumont and Young (5)):

$$G_c = \frac{P_c^2}{B_c} \frac{(1+\nu)l^2}{k_1 E W B^3} \qquad (4)$$

Once the geometrical parameters are assigned, G_c can be determined by simply measuring P_c, irrespective of a. If the fracture test is carried out at constant displacement speed, $\dot{x}$, and the load is constant during crack propagation, the crack velocity is also a constant, expressed by:

$$\dot{a} = \frac{\dot{x}}{P_c (dC/da)} \qquad (5)$$

From equations (4) and (5), under suitable experimental conditions, it thus appears possible to derive the $G_c(\dot{a})$ characteristic of the material. For a correct application of this analysis, further considerations should be made:

(i) Linear compliance actually holds good for only part of the crack length range (Trantina (6), Shetty and Virkar (7), Fuller(8)): for short cracks, the slope of the C vs. a curve is lower than the theoretical value (eq.(2)), while, for very long cracks, the slope is higher.

(ii) Since the crack front is markedly curved (Virkar and Gordon (9)), several interpretative complexities arise: the crack velocity distribution along the curved crack front calls for some

correction of the G_c or $\dot{a}$ values calculated (Pollet and Burns (10), Leevers (11), Stalder and Kausch (12), Leevers and Williams (13)).

The aim of this work is to shed more light on the requirements and limits of applicability of the above analysis to the DT test. To this end, the curved-crack growth was visualized by means of cinematographic techniques to obtain a better insight into the kinematics and dynamics of this test.

EXPERIMENTAL DETAILS

Commercial PMMA sheets were kindly supplied by VEDRIL SpA. DT specimen were machined, notched and side-grooved (side-groove depth = 0.15-0.20 B). Testing was carried out at room temperature, at a constant load-point displacement speed of 1 mm/min. Real-time visualization and recording of the crack growth was obtained with a cine or video camera. The crack was viewed perpendicularly to its plane (Fig.1b) through a metallographically-polished face of the specimen.

An example of frames is given in Fig.2. The shooting and load-recording were synchronized for the subsequent quantitative analysis.

EXPERIMENTAL RESULTS AND DISCUSSION

Statics

Static measurements of the specimen compliance, C, as a function of crack length, a, were carried out to verify the analytical relationship expressed by eq. 2 for different specimen widths, W, and thicknesses, B: deviations from linearity are normally observed at the two ends of the crack path. For crack lengths less than W/2, the torsional deformation of the two specimen halves cannot be treated as two beams under pure torsion. For crack lengths $a > L - W/2$, the uncracked portion of the plate behaves more like a bar than a plate, becoming a more compliant constraint for the two torsion beams.

For short crack-lengths, deviations from linear compliance may also stem from a thickness effect, due to the curved crack profile not being fully developed throughout the specimen's thickness: full development is reached for longer cracks in thicker specimens.

Kinematics

Two distinct stages can always be observed in the crack growth: first, the development of the crack from the initial notch through the entire thickness of the specimen, and then the "solid" translation of the crack profile along the longer axis of the plate (Fig.3). A third stage, the final abrupt break, is an end-effect and is here disregarded.

Detailed analysis of the films shows that even in stage I any subsequent crack front comes from a "solid" translation of the same profile, along a direction tilted at an angle $\emptyset$ (of 4°-7°) to the longer axis of the plate. In stage I, the crack surface A does not increase linearly with crack extension a, as it does in stage II; based on geometrical considerations it can be shown that A (a) follows a parabolic law in the first stage (Fig. 4). Thus eq. 3 holds in stage II only.

For a kinematic description of the crack growth, we may distinguish three different speeds: the nominal crack speed $\dot{a}$ along the lower edge of the specimen; the local speed $\dot{\xi}$ at a point P of the crack front, directed as its normal ξ ; and the speed $\dot{r}$ of translation of the crack profile (Fig. 3). In stage I, $\dot{r}$ is a constant (different from $\dot{a}$ in both value and direction), while the speed distribution $\dot{\xi}(P)$ varies with time, as shown in Fig.5. In the second stage, however, crack propagation takes place under stationary conditions: speed $\dot{r}$ coincides with $\dot{a}$ in both value and direction, and the local speed distribution $\dot{\xi}(P)$ does not vary with time (line d in Fig. 5).

Geometry dependence. Strain analysis has shown that both specimen geometry and material characteristics have an influence on crack-front shape (11-13).

In the present work the effect of variations in side-groove depth ($B-B_c$) was specially investigated by means of the cinematographic technique. It was found that: (i) the crack-front maintains the same shape, posture and translation direction irrespective of B_c (or groove depth), for the same specimen thickness B (Fig. 6a); (ii) the translational velocity of the crack profile ($\dot{r} = \dot{a}$ in stage II) depends on groove depth, according to eq. 5.

A variation in specimen width, W, affects the crack shape (as shown in Fig. 6b), in agreement with the findings of other authors (12, 13). The crack-front profile obtained with a modified epoxy

resin (also reported in Fig.6b) indicates the comparable effect of specimen width and material characteristics on crack shape, in agreement with Stalder and Kausch's report (12).

Dynamics

In Fig. 7, a typical load-time record, observed with a displacement-controlled machine, is compared with the corresponding crack extension diagram, drawn from the film of the fracture process.

At first, the load P rises almost linearly with time (or displacement), till the crack starts to grow (beginning of stage I). Then, the load-deflection curve bends and exhibits a maximum, after which the crack stabilizes at constant speed $\dot{a}$ (beginning of stage II) while the load keeps decreasing till it comes to a "plateau". In the end (stage III), the load drops rapidly, while the crack accelerates up to the final break.

It is worth noting that the "dynamic" steady state condition, P = const., is reached in stage II somewhat later than the "static" condition, dC/da = const., and the "kinematic" steady-state condition, $\dot{a}$ = const. This result is not inconsistent with the previous analysis, however, for, under non-stationary "dynamic" conditions eq.(5) has to be replaced by the more general expression:

$$\dot{a} = \frac{\dot{x}}{P_c(dC/da) + C(dP_c/da)} \qquad (5')$$

from which it appears that P_c can still vary even when $\dot{x}$, $\dot{a}$ and dC/da are all constant.

As pointed out by Leevers (11), if toughness is a monotonically increasing function of crack speed $\dot{a}$ (see Appendix), the constant P_c regime is in order - any change in P_c being self-correcting according to equations (4) and (5'). Our experimental data show that, in fact, the load P_c approaches a constant value during stage II. Under conditions prevailing in stage II, eq.(5') can be integrated to give a simple relationship between the (critical) load P_c and the crack extension a :

$$P_c = \frac{\dot{x}}{\dot{a}} \frac{1}{(dC/da)} + \frac{\text{const.}}{C_o/(dC/da) + a} \qquad (6)$$

in which the first term $\left[\frac{\dot{x}}{\dot{a}} \cdot \frac{1}{(dC/da)}\right]$ is the steady-state value of the (critical) load. According to eq. (6), the load P_c is expec-

ted to approach its steady-state value asymptotically.

Determination of toughness. From the force-displacement curve and the measurement of the crack surface areas in the films, an average critical strain energy release rate, G_c, at whatever stage of crack growth, a, can be determined directly from the definition:

$$G_c = \frac{dU}{dA} \tag{7}$$

as shown in Fig. 8. The value determined is an average of the energy absorbed non-uniformly along the curved crack front because of the distribution of local crack velocities, $\dot{\xi}$ (13). Fig. 9 shows an example of the curves G_c vs. a that are so determined, representing a distorted image of the resistance-curve of the material. In stage I the distribution of crack velocities, $\dot{\xi}$, varies with crack extension a (as shown in Fig.5) and that variation will influence the G_c measured. In stage II, however, the crack profile is fully established and the distribution of crack velocities, $\dot{\xi}$, no longer varies with crack propagation. The variation of G_c with a, observed in Fig. 9, which seems to reflect the behaviour of the load, cannot be so simply explained.

In the absence of this explanation, it seems advisable, in practice, to take measurements of G_c only when the load, too, reaches a constant value, i.e. when the three conditions (i) dC/da = constant (static), (ii) $\dot{a}$ = constant (kinematic), (iii) P_c = constant (dynamic), are all fulfilled. This paper shows that the crack can grow considerably before all these conditions are met: in order to achieve them, very long specimens may thus be needed.

Comparison of the G_c values obtained directly from its definition via eq. (7) and with the "compliance method" via eq. (4) shows slight but systematic differences: for example, the data shown in Fig. 7 give us G_c = 410 J/m^2 via eq. (7) and G_c= 570 J/m^2 via eq.(4).

APPENDIX

For many materials, crack resistance approximately follows an exponential dependence on crack speed. The exponent, n, can also be determined from measurements of craze stress as a function of time obtained in rate-varying tension tests (Williams and Marshall (14)). The results of this work together with literature values obtained under similar conditions are given in Table 1 hereunder :

TABLE 1

Test	Quantity measured	n	Ref.
DT	G_c - eq.(4) -	0.12	this work
DT	G_c - eq.(7) -	0.10	this work
Tensile	craze stress	0.14	this work
DT	G_c - eq.(4) -	0.12	(14)
Tensile	craze stress	0.11	(14)
DT	G_c - eq.(4) -	0.09	(6)

Acknowledgements. This work has been partly supported by the Progetto Finalizzato Chimica Fine e Secondaria, CNR, Roma.

SYMBOLS USED

a = crack length from the load plane, measured at the lower edge of the specimen (cm)

a_o = edge-notch length (cm)

a^* = crack length at the transition from stage I to stage II (cm) (see Fig.3)

$\dot{a}$ = crack velocity (mm/sec)

A = crack surface area (cm^2)

B = specimen thickness (mm)

B_c = thickness at groove (mm)

C = specimen compliance (m/N)

C_o = specimen compliance for a = 0 (eq.2) (m/N)

E = Young's modulus (MPa)

G = Shear modulus (MPa)

G_c = Strain energy release rate (KJ/m^2)

l = distance between the load points for a single beam (mm)

L = specimen length (mm)

k_1 = geometrical parameter

M_t = torsion moment (N · m)

n = crack growth exponent

P_c = critical load (KN)

$\dot{r}$ = translation velocity of crack profile (mm/sec)

t = time (sec)

U = fracture energy (J)

W = specimen width (mm)

x = cross-head displacement (mm)

x_r = translating co-ordinate (see Fig.5)

$\dot{x}$ = cross-head speed (mm/min)

θ = torsion angle (deg)

ν = Poisson's ratio

$\dot{\xi}$ = local crack velocity (mm/sec)

φ = angle between translation direction of crack profile and longer axis of the plate in stage I (deg)

REFERENCES

(1) Timoshenko, S.P., Goodier, J.N., "Theory of Elasticity", Mc Graw-Hill Book Co., New York, 1970.

(2) Kies, J.A., Clark,A.B.J., "Proceedings of the 2nd International Conference on Fracture", Brighton, 1969, p. 483.

(3) Evans, A.G., Int. J. of Frac., Vol. 9, 1973, pp.267-275.

(4) Marshall G.P., Coutts, L.H., Williams, J.G., J. of Mat. Sci., Vol. 9, 1974, pp. 1409-1419

(5) Beaumont, P.W.R., Young, R.J., J. of Mat. Sci., Vol. 10, 1975, pp. 1334-1342.

(6) Trantina, G.G., J. of Am.Cer.Soc., Vol. 60, 1977, pp. 338-341.

(7) Shetty, D.K., Virkar, A.V., J. of Am.Cer.Soc., Vol. 61, 1978, pp. 93-94.

(8) Fuller, E.R., Jr., "Fracture Mechanics Applied to Brittle Materials", ASTM STP 678, S.W.Freiman ed., 1979, pp.3-18.

(9) Virkar, A.V., Gordon, R.S., J. of Am.Cer.Soc., Vol. 58, 1975, pp. 536-537.

(10) Pollet, J.C., Burns, S.J., J. of Am.Cer.Soc., Vol. 62, 1979, pp. 426-427.

(11) Leevers, P.S., J. of Mat. Sci., Vol. 17, 1982, pp.2469-2480.

(12) Stalder B., Kausch, H.H., J. of Mat. Sci., Vol. 17, 1982, pp. 2481-2485.

(13) Leevers, P.S., Williams, J. G., J. of Mat.Sci., Vol. 20, 1985, pp. 77-84.

(14) Williams, J.G., Marshall, G.P., Proc. R. Soc. London, A.342, 1975, p. 55.

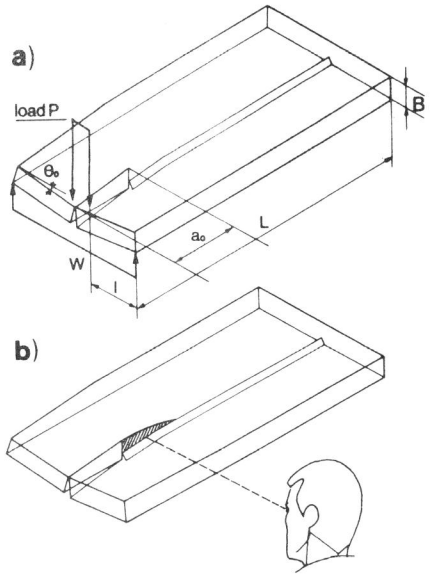

Figure 1 a) DT specimen under test conditions
b) crack growth visualization

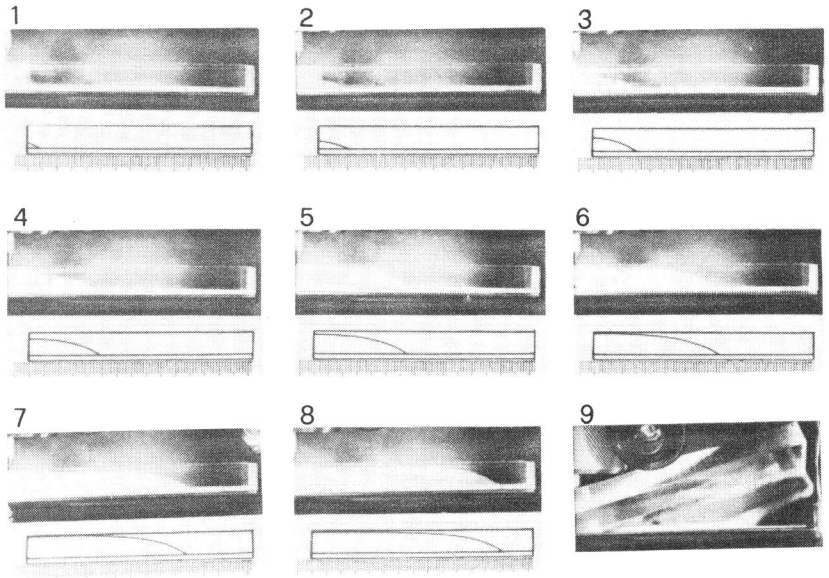

Figure 2 Frames illustrating crack propagation (Δt = 4 sec) for a 12x50x120 mm specimen (One division = 6 mm).

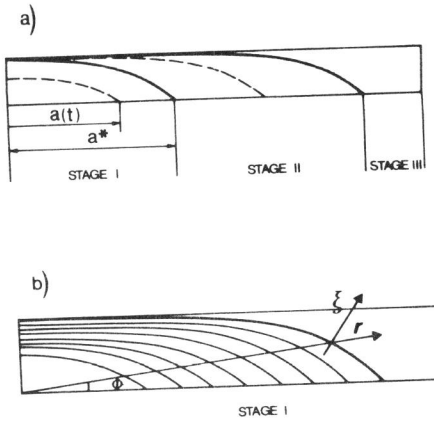

Figure 3 a) Different stages in crack propagation; b) crack fronts in stage I.

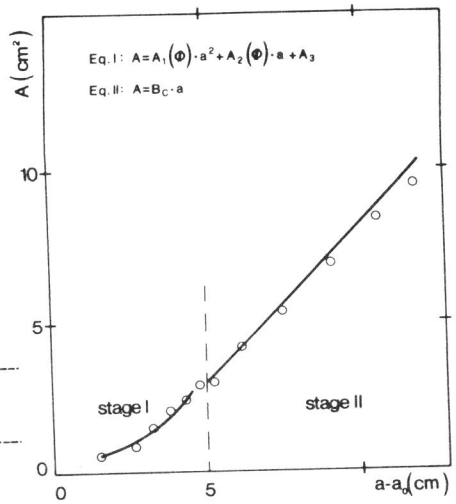

Figure 4 Fracture surface area versus crack length: (o) experimental data, (—) predicted values from Eq. I and Eq. II.

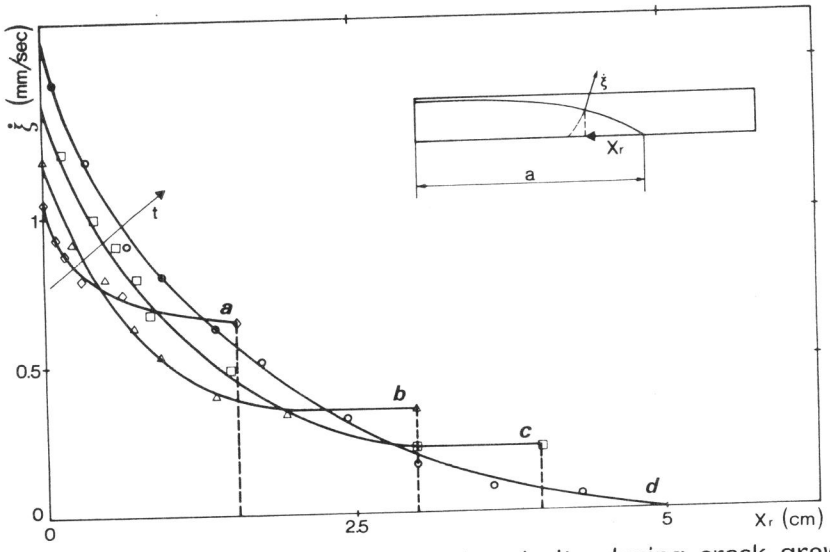

Figure 5 Distribution of local crack velocity during crack growth for a 12x50x200 mm specimen (a,b,c,d correspond to Δt = 5 sec).

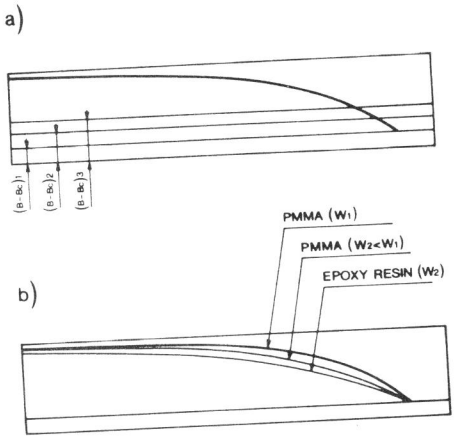

Figure 6 Crack profiles: a) for different side-groove depths, b) for different materials and specimen widths.

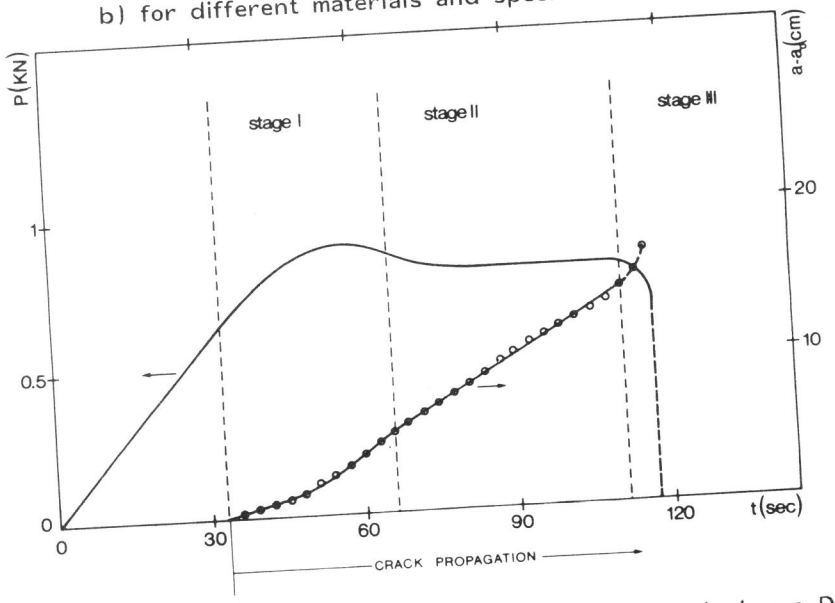

Figure 7 Load and nominal crack length versus time during a DT test. (Specimen sizes: 12x50x200 mm).

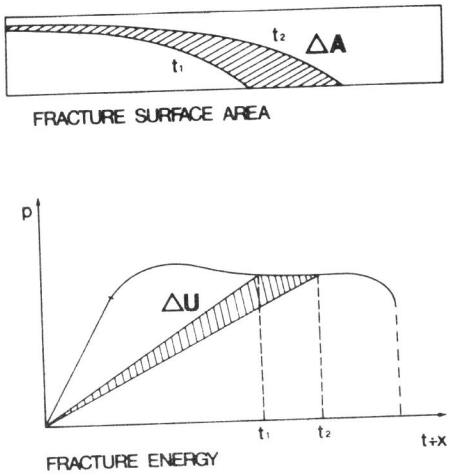

Figure 8 Diagram showing method of determinating fracture surface area and fracture energy.

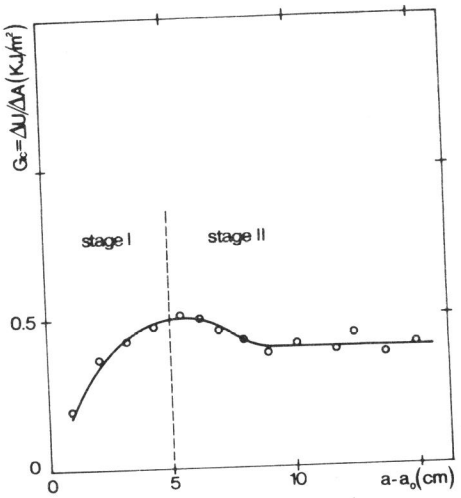

Figure 9 G_c values (according to eq. 7) versus crack length for a 12x50x200 mm specimen.